Improving pre-salt targets using wave-equation velocity analysis

Daniela Donno, Sergio Barragan, Florian Jouno, Adel Khalil, CGG

Abstract

Despite continuous improvements in model-building technologies, imaging below salt remains challenging. Reflection full-waveform inversion (RFWI) is effective at providing low-wavenumber velocity updates beyond the penetration depth of diving waves, however it is still susceptible to amplitude mismatch between input and modeled data. It also suffers from limitations imposed by narrow-azimuth (NAZ) seismic acquisition. To reduce the adverse impact of amplitude differences between input and modeled data, we present here a stack-power wave-equation migration velocity analysis (WEMVA) method. Differently than RFWI, this method uses an objective function defined in the image domain. Therefore, it depends more on the kinematic part of the propagated wavefields, resulting in a more reliable inversion scheme. We also introduce a regularization term that reduces the footprints created in the velocity updates by NAZ seismic data. We demonstrate the effectiveness of this method by using synthetic and field data with NAZ acquisition geometries. Finally, we discuss some of its limitations, and suggest ideas for further improvements.

Introduction

Full-waveform inversion (FWI) has become a standard method for velocity model building. Within the diving-wave penetration depth, it resolves a wide variety of complex geological features. Below the diving-wave penetration depth, the inversion is driven by reflections, which exhibit stronger nonlinearities that can adversely affect the inversion. Notwithstanding, several works have achieved promising results on real data using reflections in the framework of reflection FWI (RFWI) (e.g., Xu et al., 2012; Irabor & Warner, 2016; Sun et al., 2016; Gomes & Chazalnoel, 2017). The common idea of most RFWI approaches is to iterate between the computation of the migration term and the tomographic term, where the migration term is used to model synthetic reflected data and the tomographic term allows updating the velocity model.

A common difficulty for RFWI methods is the amplitude mismatch between real data and modeled synthetic data, which can negatively impact the computation of the data residual and consequently the velocity gradient. One possible strategy to partly mitigate this problem is to use cross-correlation-based cost functions (Xu et al., 2012; Brossier et al., 2015) or travel-time cost functions that minimize the time shifts between input and modeled synthetic data (Luo & Schuster, 1991). Another possibility is to use image-based objective functions such as wave-equation migration velocity analysis (WEMVA) methods (Symes, 2008), which depend more on the kinematic part of the propagated wavefields. The kinematics of the forward modeled data, which are used to compute the image and velocity gradient, are relatively more robust and can better represent the model; therefore, an objective function in the image domain should allow for a more reliable inversion of field data.

WEMVA methods can be mainly separated into two categories. One category minimizes the action of an annihilator on the extended images (e.g., Symes & Carazzone, 1991) and the other one maximizes the image semblance or coherence (Soubaras & Gratacos, 2007). The methods that use extended images have generally more convex cost functions than those that maximize the image semblance (Symes, 2008). However, artifacts in the extended images are well known to damage the gradient and the inversion convergence (Fei & Williamson, 2010; Mulder, 2014; Lameloise et al., 2015). Another advantage of the image stack-power WEMVA method (Soubaras & Gratacos, 2007) is its computational cost, which is comparable to that of RFWI.

In this paper, we present a stack-power WEMVA approach and introduce a regularization term that reduces the footprint of narrow-azimuth (NAZ) towed-streamer acquisition geometry upon the velocity updates. We illustrate the effectiveness of this approach with a 3D synthetic example as well as with a field dataset with a NAZ acquisition geometry from the Santos basin, offshore Brazil.

Method

The WEMVA method that we present here seeks a model $\mathbf{m}$ that maximizes the following objective function

$$\chi(\mathbf{m}) = \chi_I(\mathbf{m}) - \alpha\chi_R(\mathbf{m}), \quad (1)$$

where $\chi_I(\mathbf{m})$ is the image-based objective function, $\chi_R(\mathbf{m})$ is a regularization term that alleviates the NAZ acquisition footprints, and α is a parameter that balances the contributions between the image and regularization terms.

The image term $\chi_I(\mathbf{m})$ is defined as the image stack-power (Soubaras & Gratacos, 2007)

$$\chi_I(\mathbf{m}) = \frac{1}{2}\sum_{\mathbf{x}} \|I(\mathbf{x}|\mathbf{m})\|^2, \quad (2)$$

where $\mathbf{x} = (x, y, z)$ represents the 3D image coordinates and the image $I(\mathbf{x})$ is formed by summing the cross-correlation of the source forward wavefield S from all the shots s with the back-propagated data wavefield D injected at the receiver locations. Equation 2 is optimized using gradient-based methods. The gradient, computed with the adjoint-state method (Plessix, 2006), can be written as:

$$G(x) = \sum_{s,r} \int_0^T \frac{2}{v^3} \left[\frac{\partial^2 S(\mathbf{x},t)}{\partial t^2} \tilde{D}(\mathbf{x},t) + \frac{\partial^2 D(\mathbf{x},t)}{\partial t^2} \tilde{S}(\mathbf{x},t) \right] dt, \quad (3)$$

where the adjoint wavefields $\tilde{S}$ and $\tilde{D}$ are source and receiver scattered wavefields which are computed through Born modeling. It is interesting to note that, the gradient in equation 3 bears resemblance to the gradient of the demigration-based RFWI (Xu et al., 2012). The difference is that in the demigration-based RFWI the back-propagated measurements are the residuals between input data and the Born modeled synthetic data.

The regularization term $\chi_R(\mathbf{m})$ is defined as

$$\chi_R(\mathbf{m}) = \frac{1}{2} \| \boldsymbol{R}_x (\mathbf{m} - \mathbf{m}_0) \|^2, \quad (4)$$

where $\mathbf{m}_0$ is the starting model and $\boldsymbol{R}_x$ is a spatial filter operator along the acquisition (inline) direction x, that mitigates the footprints generated by the poorly sampled NAZ acquisition.

Synthetic example

To illustrate the effect of the regularization term, we consider a 3D synthetic example created with a NAZ geometry with 500 m sail-line spacing. The receiver spread utilizes ten 8 km cables separated by 100 m. The channel spacing is 50 m and the shot spacing is 150 m. Figures 1a and 1c depict an inline section of the 3D velocity and density models used to create our observed data. This velocity model (Figure 1a) represents a typical geology of deep-water Santos basin, offshore Brazil. It is characterized by a water-bottom around 2.4 km depth and a thick block of dirty salt (greenish color), which separates the post-salt sediments (above salt) from the pre-salt sediments (below salt). For the starting velocity model, we added a ± 200 m/s checkboard perturbation, between 7.5 and 8.5 km depth (Figure 1b), in the pre-salt region, where the largest Brazilian reservoirs are usually located.

Figure 2a shows a depth slice at 8 km depth of the perturbation that we want to retrieve. The size of each perturbation block is 2 km x 2 km. Figure 2b is the velocity update using the stack-power WEMVA objective function (equation 2). We can note that this update is affected by footprints oriented along the acquisition (inline) direction (i.e. in the black dashed box in Figure 2b). The result of Figure 2c is obtained when including the regularization term as in equation 1. We note that the footprints are reduced and the perturbation resembles more the actual checkboard (Figure 2a). We can also note that there is a scale difference between the two perturbations of Figures 2b and 2c, with the values of the velocity update with regularization (Figure 2c) being much closer to the true values. This is because the gradient obtained with the regularization is closer to the true perturbation and it allows the algorithm to converge more than in the case without regularization.

We repeated this experiment also using a wide-azimuth (WAZ) acquisition geometry, whose main difference with respect to the NAZ geometry is that, for each shot, the receiver patch measures 8 km in the inline direction and 4 km in crossline. The results of the velocity updates using the stack-power WEMVA without and with the regularization term are shown in Figures 2d and 2e, respectively. As expected, the velocity update using WAZ data (Figure 2d) does not suffer from strong acquisition footprints. The use of the regularization term is less necessary in this case, even though the result with regularization (Figure 2e) is slightly better than the one without regularization (Figure 2d).

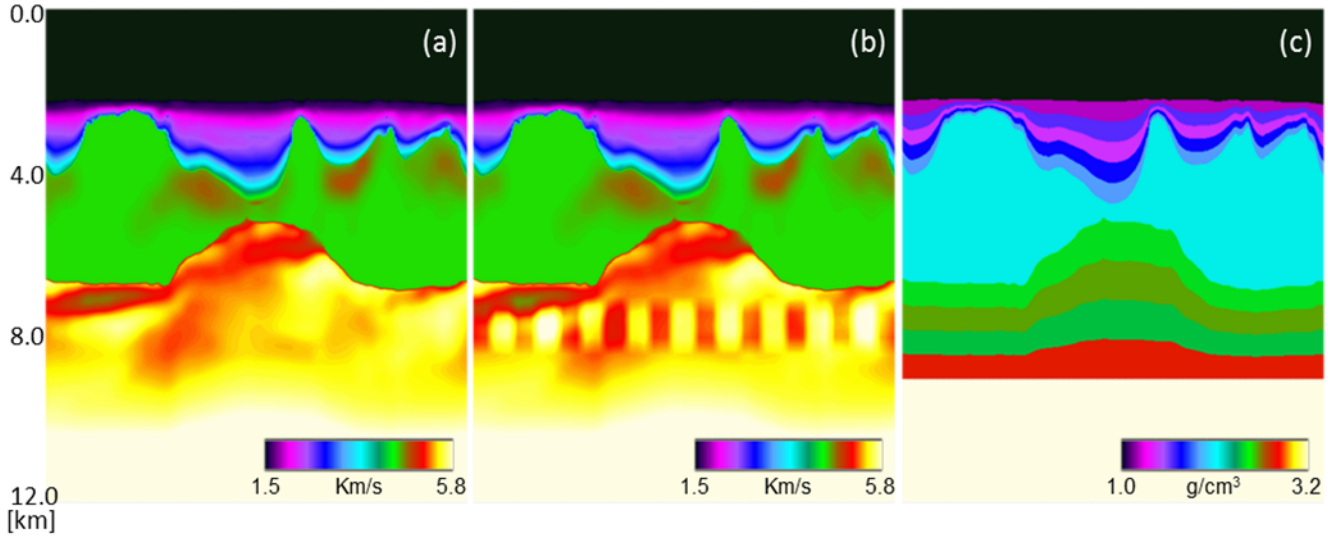

Figure 1 – *Synthetic example: inline section of (a) input velocity model, (b) perturbed velocity model, (c) density model used to generate the synthetic observed data.*

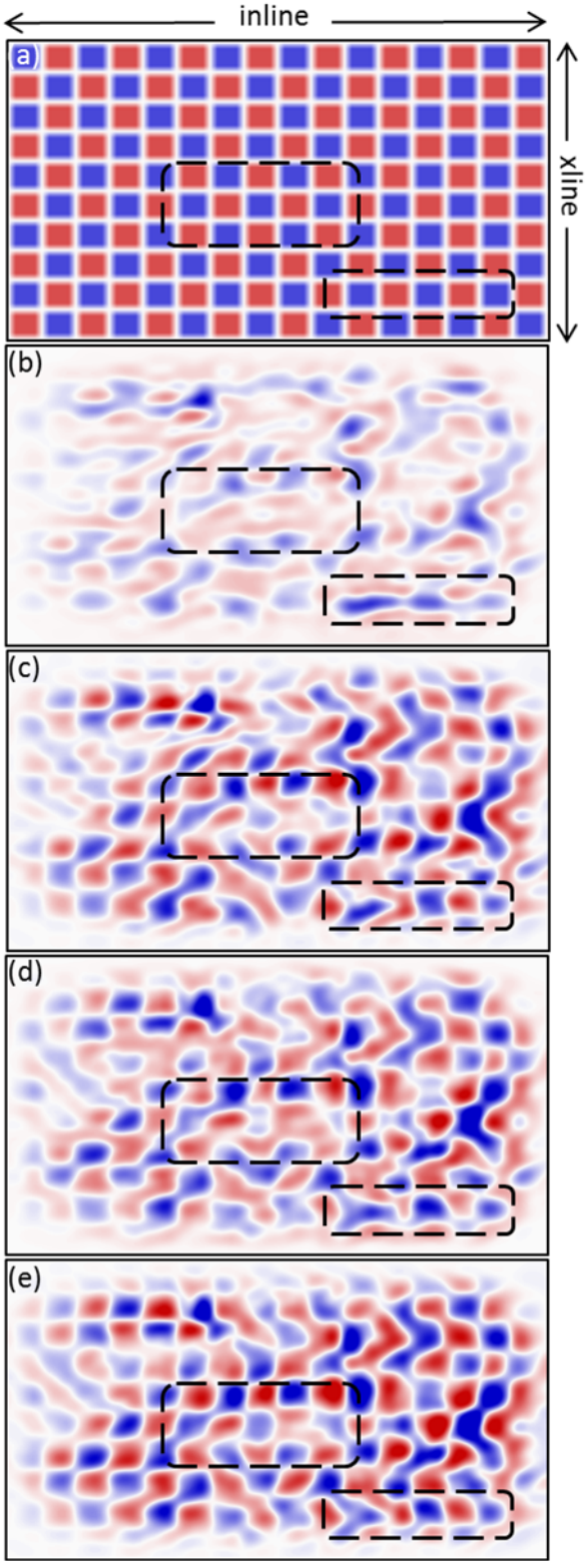

Figure 2 – *Synthetic example: depth slice at 8 km depth of a) the actual velocity perturbation, b-c) the velocity update using the stack-power WEMVA with NAZ data, without and with regularization respectively, d-e) the velocity update using the stack-power WEMVA with WAZ data, without and with regularization, respectively.*

It is well known that reflection-based wave-equation velocity analysis techniques like RFWI and WEMVA are susceptible to inadequate illumination (Gomes & Yang, 2018), especially in the presence of complex overburden (as analyzed with more details in the Discussion section). This is visible here when comparing the checkboard pattern between the NAZ and WAZ surveys, with the latter showing greater ability for resolving a more accurate response.

Field data example

The field data are from a deep-water survey over Santos basin, offshore Brazil. The water depth ranges from about 2400 m to 2800 m. The seismic data were acquired using a NAZ acquisition configuration with variable-depth streamers, maximum offset of 8.2 km along the cables and 1.1 km across the cables.

The initial velocity model was obtained after several iterations of ray-based reflection tomography, diving-wave conventional FWI and time-lag FWI (Zhang et al., 2018) for the post-salt sediments, followed by salt interpretation and pre-salt velocity updates. The data pre-processing for the stack-power WEMVA includes denoise, source and receiver deghosting, designature, surface-related multiple elimination and shot-domain regularization. Moreover, the transmitted energy of the input data is muted so as to use only reflected energy.

Stack-power WEMVA was performed from 5 to 7 Hz. The strategy of starting from the lower frequency in the data and going towards higher frequencies, similar as in conventional FWI (Bunks et al., 1995), allows to overcome the multimodality issue, as proposed by Soubaras & Gratacos (2007). Moreover, a scheme was implemented that optimized the cost function for the region of interest such that we were able to focus the velocity updates mostly in the salt and pre-salt regions.

Figures 3a and 4a show the input velocity model overlaid on the reverse time migration (RTM) stack for two cross sections. RTM stack images and Kirchhoff common image gathers (CIGs) for the initial velocity model are displayed in Figures 3b-c and 4b-c. We can observe that, due to the complexity of the overburden, with carbonate layers, volcanic intrusions and complex salt geometries (Figure 3b), the pre-salt events are poorly imaged (yellow arrows in Figure 3b) and the base-of-salt (BOS) event is not always visible (Figure 4b).

After the velocity update using stack-power WEMVA (Figure 3d and 4d), we can observe several improvements in the BOS continuity and in the focusing of the deeper pre-salt events, both in the migrated images and in the gathers (Figures 3e-f and 4e-f).

Discussion and limitations

We have shown that the velocity update obtained with the stack-power WEMVA can help in improving the imaging

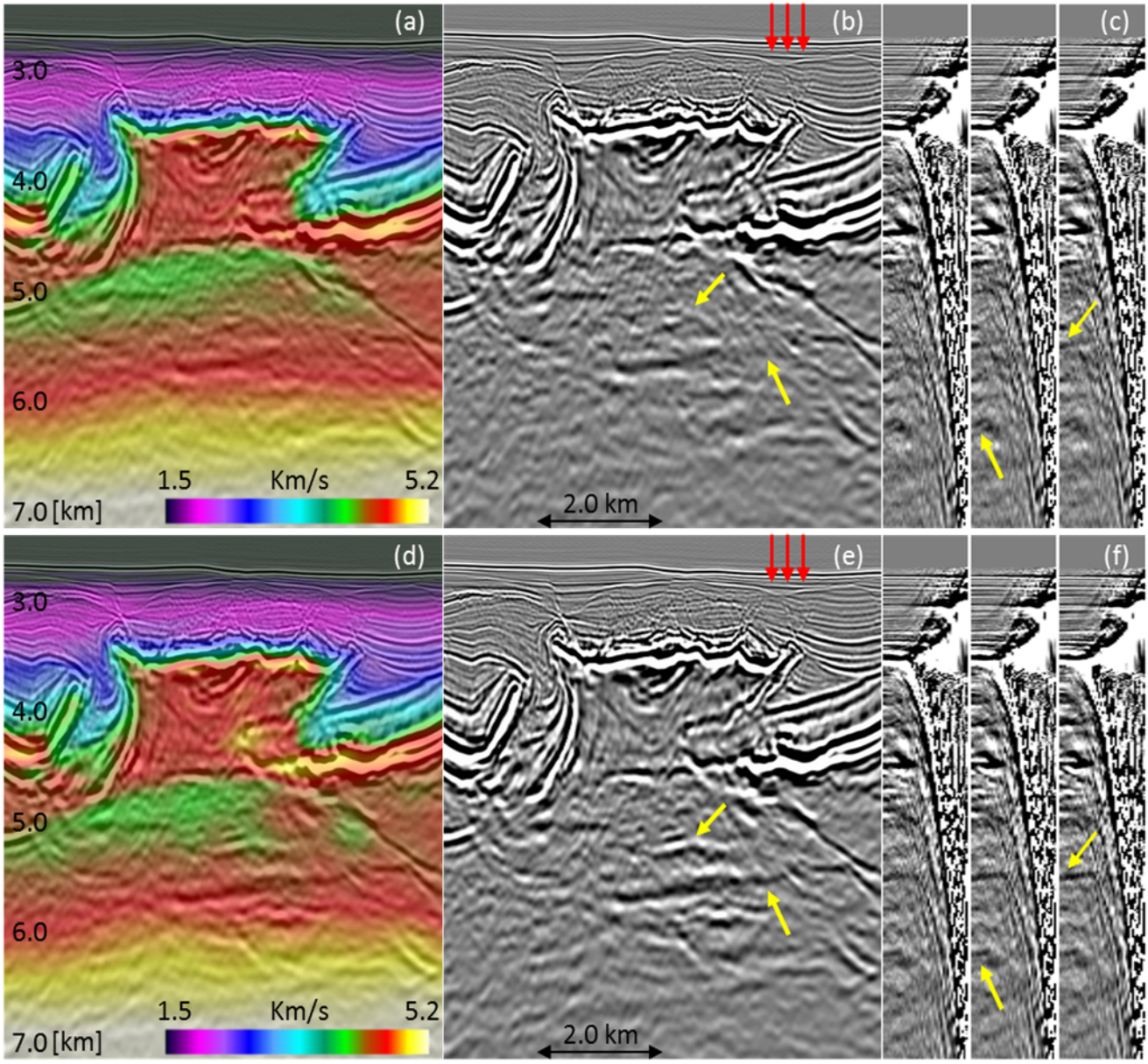

Figure 3 – *Section of field data before the stack-power WEMVA update: (a) initial velocity model overlaid on the RTM stack, (b) RTM stack, (c) Kirchhoff CIGs. Section after the stack-power WEMVA update: (d) updates velocity model overlaid on the RTM stack, (e) RTM stack, (f) Kirchhoff CIGs. The red arrows indicate the location of the CIGs. The yellows arrows indicate places where the stack image and the gathers are improved.*

of deep areas, beyond the penetration depth of diving waves. However, there are still some limitations that need to be addressed.

For NAZ data, we have proposed a regularization term (equation 4) that reduces the strong footprints along the acquisition direction, which are generated by the poor inline sampling from NAZ data. Nonetheless, the velocity update for NAZ data obtained when using the regularization term (Figure 2c) is not as good as that obtained with WAZ data (Figure 2d-e). In particular, we focus attention on the area with distorted velocity update within the black dashed rectangle in Figure 5a (same result of Figure 2c). We notice that this area in the pre-salt corresponds to a very shallow top of salt (Figure 5b). This observation reveals that, for NAZ data, the velocity updates are affected not only by the acquisition footprints that can be mitigated with the proposed regularization term, but also by illumination variations related with the presence of complex overburden. Reduction of the imprint of the illumination variations could be achieved using a least-squares reflectivity image (Wang et al., 2016; Gomes & Yang, 2018), and through a better approximation of the Hessian matrix in the velocity inversion phase (Métivier et al., 2013).

Finally, the presence of strong internal multiples in the data and in the reflectivity used for the Born modeling might bias the velocity update (Mulder, 2008). Therefore, this is another issue to take care of, especially in the

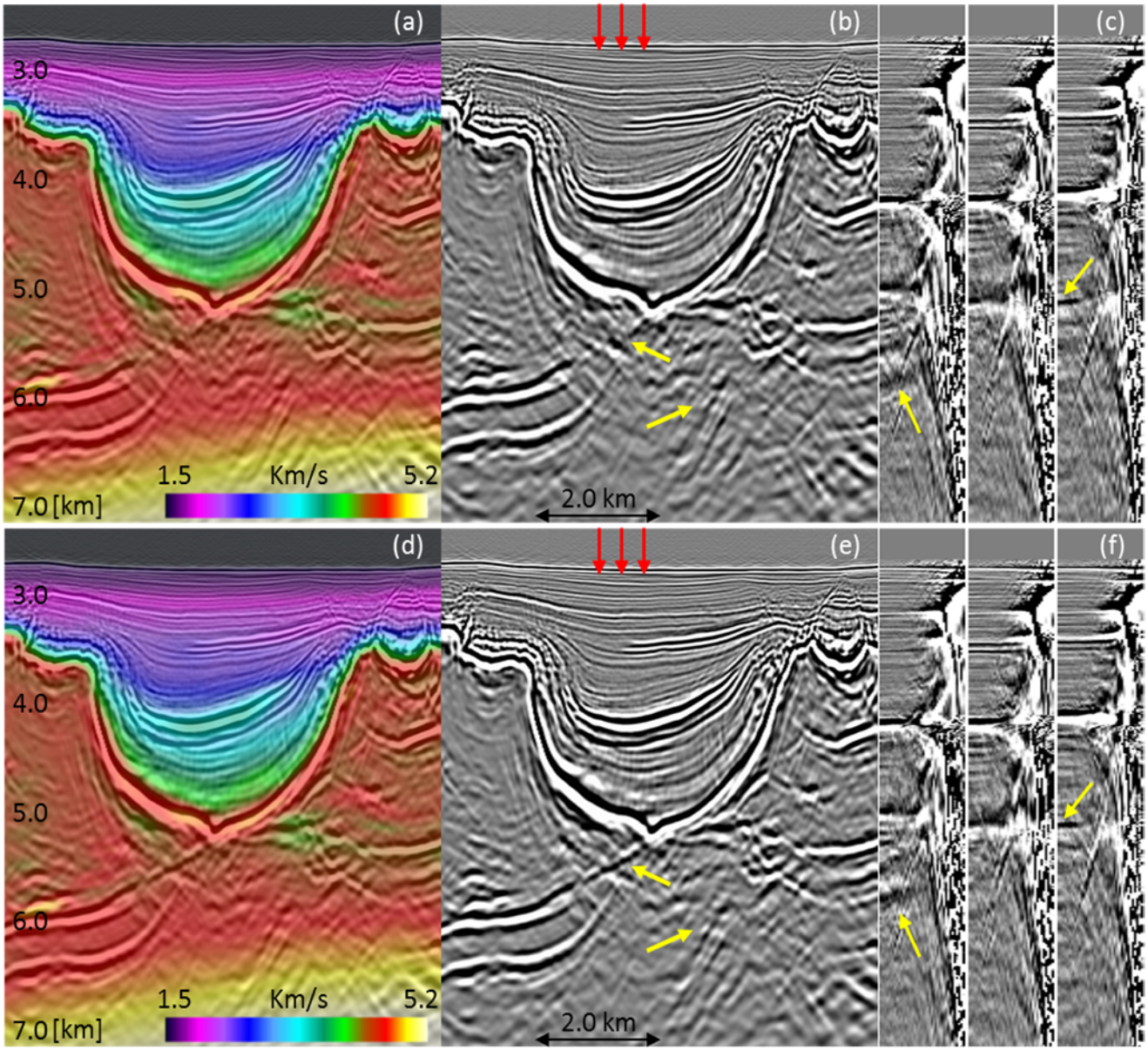

Figure 4 *– Cross section of field data before the stack-power WEMVA update: (a) initial velocity model overlaid on the RTM stack, (b) RTM stack, (c) Kirchhoff CIGs. Cross section after the stack-power WEMVA update: (d) updates velocity model overlaid on the RTM stack, (e) RTM stack, (f) Kirchhoff CIGs. The red arrows indicate the location of the CIGs. The yellows arrows indicate places where the stack image and the gathers are improved.*

Santos basin where the presence of strong internal multiples is a well-known problem (Krueger et al., 2018).

Conclusions

The presented stack-power WEMVA approach has the advantage of using an objective function defined in the image domain that is less dependent on amplitude matching between input and modeled data. Moreover, the use of a regularization term allows mitigation of the impact of footprints created in the velocity update when using NAZ seismic data.

Results of the application of this method on a field NAZ dataset from deep-water offshore Brazil look promising. Some challenges still need to be addressed, and the need for WAZ data is irreplaceable.

Acknowledgments

The authors would like to thank CGG for the permission to publish this work and CGG Multi-Client & New Ventures for the Santos basin data set.

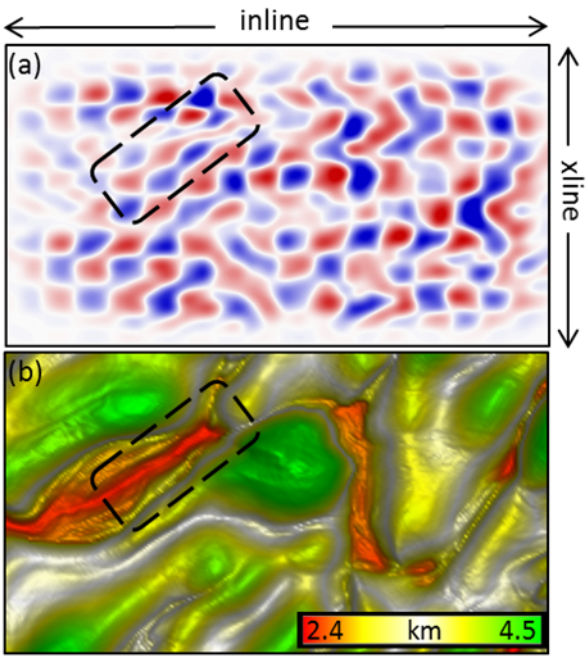

Figure 5 – *Synthetic example: a) Depth slice at 8 km depth of the velocity update using the regularized stack-power WEMVA with NAZ data (same as Figure 2c); b) Top-of-salt horizon in the same area. The black dashed rectangles indicate an area where the velocity updates are affected by illumination variations related with the complex overburden, having a very shallow top of salt (only few hundreds of meters below the water bottom).*

References

BROSSIER, R., S. OPERTO & J. VIRIEUX, Velocity model building from seismic reflection data by full-waveform inversion: Geophysical Prospecting, 63, 354–367, 2015.

BUNKS, C., F. M. SALECK, S. ZALESKI & G. CHAVENT, Multiscale seismic waveform inversion: Geophysics, 60, 1457–1473, 1995.

FEI, W. & P. WILLIAMSON, On the gradient artifacts in migration velocity analysis based on differential semblance optimization: 80th Annual International Meeting, SEG, Expanded Abstracts, 4071–4076, 2010.

GOMES, A. & N. CHAZALNOEL, Extending the reach of FWI with reflection data: Potential and challenges: 87th Annual International Meeting, SEG, Expanded Abstracts, 1454–1459, 2017.

GOMES, A. & Z. YANG, Improving reflection FWI reflectivity using LSRTM in the curvelet domain: 88th Annual International Meeting, SEG, Expanded Abstracts, 1248–1252, 2018.

IRABOR, K. & M. WARNER, Reflection FWI: 86th Annual International Meeting, SEG, Expanded Abstracts, 1136–1140, 2016.

KRUEGER, J., D. DONNO, R. PEREIRA, D. MONDINI, A. SOUZA, J. ESPINOZA & A. KHALIL, Internal multiple attenuation for four pre-salt fields in the Santos Basin, Brazil: 88th Annual Meeting, SEG, Expanded Abstracts, 4523–4527, 2018.

LAMELOISE, C.-A., H. CHAURIS & M. NOBLE, Improving the gradient of the image-domain objective function using quantitative migration for a more robust migration velocity analysis: Geophysical Prospecting, 63, 391–404, 2015.

LUO, Y. & G. T. SCHUSTER, Wave-equation traveltime inversion: Geophysics, 56(5), 645-653, 1991.

MÉTIVIER, L., R. BROSSIER, J. VIRIEUX & S. OPERTO, Full waveform inversion and the truncated Newton method: SIAM Journal on Scientific Computing, 35(2), B401-B437, 2013.

MULDER, W. A., Automatic velocity analysis with the two-way wave equation: 70th Annual International Conference and Exhibition, EAGE, Extended Abstracts, P165, 2008.

MULDER, W. A., Subsurface offset behaviour in velocity analysis with extended reflectivity images: Geophysical Prospecting, 62, 17–33, 2014.

PLESSIX, R.-E., A review of the adjoint-state method for computing the gradient of a functional with geophysical applications: Geophysical Journal International, 167(2), 495–503, 2006.

SOUBARAS, R. & B. GRATACOS, Velocity model building by semblance maximization of modulated-shot gathers: Geophysics, 72(5), U67–U73, 2007.

SUN, D., K. JIAO, X. CHENG & D. VIGH, Reflection based waveform inversion: 86th Annual International Meeting, SEG, Expanded Abstracts, 1151–1156, 2016.

SYMES, W. W., Migration velocity analysis and waveform inversion: Geophysical Prospecting, 56, 765–790, 2008.

SYMES, W. W. & J. J. CARAZZONE, Velocity inversion by differential semblance optimization: Geophysics, 56, 654–663, 1991.

WANG, F., D. DONNO, H. CHAURIS, H. CALANDRA & F. AUDEBERT, Waveform inversion based on wavefield decomposition: Geophysics, 81(6), R457-R470, 2016.

XU, S., D. WANG, F. CHEN, Y. ZHANG & G. LAMBARÉ, Full waveform inversion for reflected seismic data: 74th Annual International Conference and Exhibition, EAGE, Extended Abstracts, W024, 2012.

ZHANG, Z., J. MEI, F. LIN, R. HUANG & P. WANG, Correcting for salt misinterpretation with full-waveform inversion: 88th Annual International Meeting, SEG, Expanded Abstracts, 1143-1147, 2018.